GEOLOGICA CARPATHICA, 48, 5, BRATISLAVA, OCTOBER 1997
303–313

U-Au-Co-Bi-REE MINERALIZATION IN THE GEMERIC UNIT (WESTERN CARPATHIANS, SLOVAKIA)

IGOR ROJKOVIČ[1], MILAN HÁBER[2] and LADISLAV NOVOTNÝ[3]

[1]Faculty of Sciences, Comenius University, Mlynská dolina, 842 15 Bratislava, Slovak Republic
[2]Geological Institute, Slovak Academy of Sciences Bratislava, Branch: Severná 5, 974 01 Banská Bystrica, Slovak Republic
[3]URANPRES, Spišská Nová Ves, Slovak Republic

Project No. 373

(Manuscript received November 28, 1996; accepted in revised form March 18, 1997)

Abstract: Uranium mineralization occurs in a quartz vein with gold and REE minerals. The vein cuts the Early Paleozoic rocks in the proximity of the granite body of the Humel Massif. The mineralization is represented by uraninite, brannerite, arsenopyrite, pyrite, glaucodot, gold, galena, bismuth, bismuthinite, xenotime-(Y), rutile, sericite, chlorite, apatite, monazite-(Ce) and tourmaline. Secondary minerals are represented by goethite, trögerite, zeunerite and scorodite.

Key words: Gemeric Unit, Early Paleozoic, quartz vein, U-Au-Co-Bi-REE minerals, element association.

Introduction

The mineralization was found 5.3 km south of Prakovce village and 1.6 km east of Ovčinec Hill 1011.7 m, 100–200 m north from main range of the Slovenské rudohorie Mts., at the end of Zimná Voda Valley (Fig. 1). Gold was found in 1975 (Novotný & Čížek 1979) during prospecting for uranium mineralization. Detailed prospecting for gold was made in 1992–95. Uranium mineralization associated with gold was also found near Hnilec Granite in the Peklisko locality (Rojkovič & Novotný 1993).

Geological setting

The Early Paleozoic rocks are represented mostly by phyllites and metatuffs of rhyolite in the area studied. Sediments are represented by quartz-(chlorite)-sericite phyllite, metaquartzite, black phyllite and lydite. They belong to the Silurian Bystrý Potok Formation of the Gelnica Group underlying the Devonian Rakovec Group (Bajaník et al. 1981; Bajaník et al. 1984; Ivanička et al. 1989). The Gelnica Group of the Gemeric Unit is characterized by a polygenetic and polycyclic sedimentary history. It was formed by mesorhythmic sedimentation of sandstone and claystone accompanied by acid volcanism (Vozárová & Ivanička 1993). The age of the volcanism according to U-Pb dating of zircon from metarhyolite is 403 Ma (Cambel et al. 1990). The upper parts of the mesorhythms contain carbonates and lydite. According to Grecula (1982), the Gelnica and Rakovec Groups represent a synchronous development of the Early Paleozoic sedimentary basin in the Volovec Group divided into the Betliar, Smolník and Hnilec Formation and surrounding rocks of the mineralization studied belong to the Betliar Formation of the Humel Nappe. The Early Paleozoic sequences are metamorphosed mostly in the chlorite zone of the green schist facies (Faryad 1991). The Gemeric Granite intruded into these sequences. They are from 270 to 246, or 223 Ma old according to Rb-Sr dating (Kovách et al. 1986; Cambel et al. 1990).

The quartz vein was found in two outcrops in a distance of 250 m from each other. The rocks in places underwent contact metamorphism affected (Faryad 1991) by near (ca. 600 m) apophysis of the Humel Massif Granite (Figs. 1, 2).

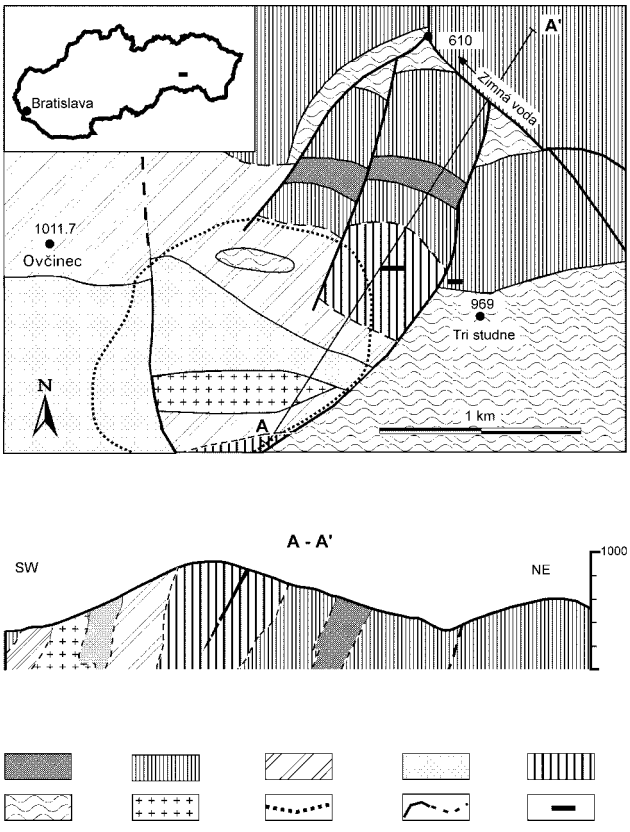

Fig. 1. Localization of Zimná Voda. Geology adapted after Bajaník et al. (1984): **1** — metalydite, **2** — black phyllite, **3** — quartz-sericite phyllite with black phyllite, **4** — metatuffite of rhyolite, **5** — metaquartzwacke with quartz phyllite and quartzite, **6** — coarse-grained metaquartzwacke, **7** — Humel Granite Massif, **8** — zone of contact metamorphosed rocks, **9** — faults, **10** — outcrops of vein.

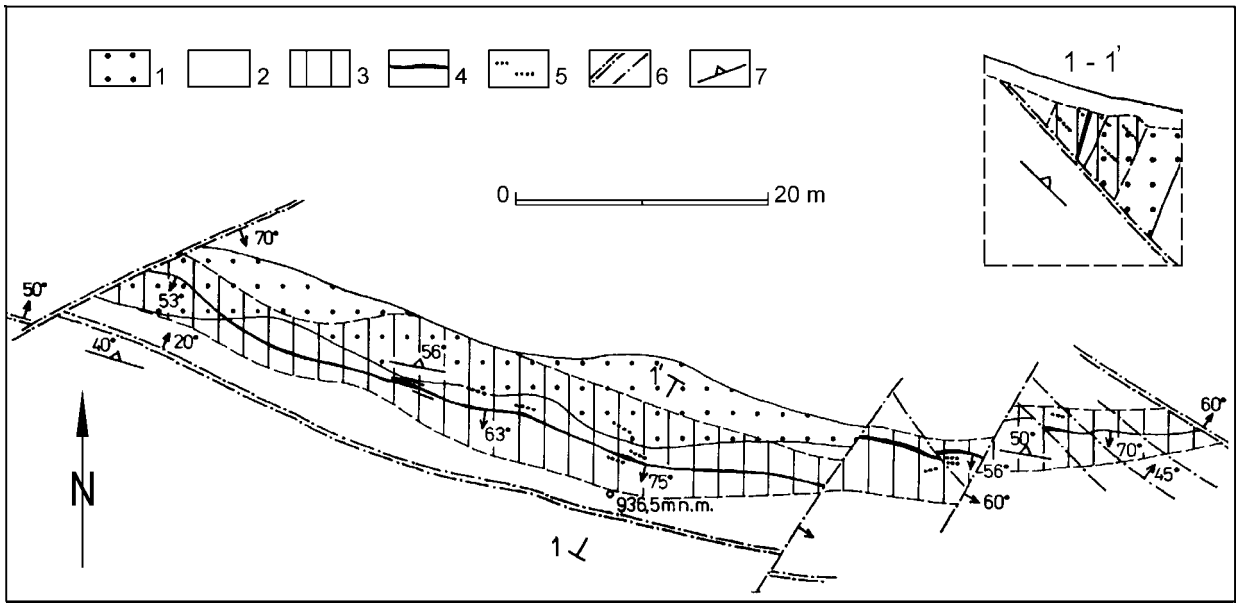

Fig. 2. Western section of the vein. **1** — metaquartzite, **2** — phyllite, **3** — altered rock, **4** — ore vein, **5** — secretion veins, **6** — fault, **7** — cleavage.

U-Au mineralization is bound to parallel veinlets forming stockwork up to 1 m thick, with an E-W direction, dipping 60–80° to the south in an outcrop with a length of only 30 m in the eastern occurrence of the vein. Wall rocks are represented by closer grey-green psammitic phyllite and by sericitic metaquartzite. Veinlets from 1 to 5 cm across are formed by fine-grained brownish quartz with disseminated uraninite or torbernite.

The vein was confirmed by trenches in the length of 83 m in the western part. Beyond this, it is cut by faults and its continuation was not found yet. The vein is cut in depth of 5–15 m by parallel fault as was confirmed by shallow drilling. The extension of displacement in the underlying part of the vein is not known (Fig. 2). The dominant wall rock is light green sericitic phyllite with local light green fine-grained sericitic metaquartzite or greenish-grey metagreywacke. Its schistosity dips from 40° to 60° towards the north. The quartz vein with an E-W direction dips 60–75° towards the south, and measures from 5 to 30 cm across (10 cm in average). The ore minerals including gold form irregular small local accumulations or high-grade sections from 1 to 2 metres long in fine-grained quartz of brown colour.

The vein is accompanied by zone of alteration from 2 to 8 m wide represented by silicification and pyritization. Short quartz veinlets of white colour from 5 to 15 cm across oriented in conformity with the schistosity of the rocks also occur in this zone. This quartz is accompanied only by rare pyrite. Au content in these veinlets varies from 0.17 to 0.51 ppm in distance up to 2 m from the main vein.

Methods used

The radioactivity of uranium minerals enables easy localization of the vein and sampling of high-grade uranium ore containing gold. Polished sections for X-ray microanalysis and thin sections were made. Ore and rock-forming minerals were studied by polarized microscope in transmitted as well as in reflected light and by scanning electron microscope (SEM). Distribution and textures of minerals were studied in vein as well as in wall rock. They were analyzed by wave-dispersion X-ray microanalysis (WDX), energy-dispersion X-ray microanalysis (EDX) and by X-ray diffraction analysis (XRD). Quantitative analyses of minerals were made by the JEOL JXA-733 Superprobe and KEVEX DELTA using voltage 20 kV, current 20 nA(WDX) and 1.2 nA (EDX), beam diameter 3–5 μm. All analyses were corrected by ZAF-correction of Kevex Sesame and Kevex Quantex software. Metal, sulphides and oxides of similar chemical composition were used as standards.

The following analytical methods were used for geochemical characteristic of mineralization:
— chemical wet analysis and X-ray fluorescence analysis (XFA) for major and minor elements of the rocks,
— P_2O_5 by colorimetry,
— Rock-Eval pyrolysis for C_{org},
— atomic emission spectroscopy with induction coupled plasma (AES-ICP) for the rare earth elements (REE),
— optical emission spectroscopy (OES) for the others elements.

Mineralogical characteristic

Uranium minerals and gold disseminated in brownish quartz are visible to the naked eye in some places in the vein. Uraninite, brannerite and arsenopyrite are the main ore minerals disseminated in fine-grained quartz. They are accompanied by pyrite, glaucodot, gold, galena, bismuth, bismuthinite, tetrahedrite, molybdenite, xenotime-(Y), monazite-(Ce), rutile, sericite, chlorite, apatite and tourmaline.

Uraninite UO_2 is the main uranium mineral. Its surface is often rough and porous. It forms colloform botryoidal aggregates or concentric zonal aggregates (around 1 mm across) vis-

ible macroscopically (Figs. 3, 4). Synaeresis fissures can often be observed. Uraninite is closely associated with brannerite. Concentric colloform aggregates are rimmed, enclosed and filled with younger brannerite, xenotime-(Y), pyrite and arsenopyrite (Fig. 5). WDX analysis has confirmed besides uranium presence of Pb, Fe, Si, Ca and Ti in uraninite (Table 1).

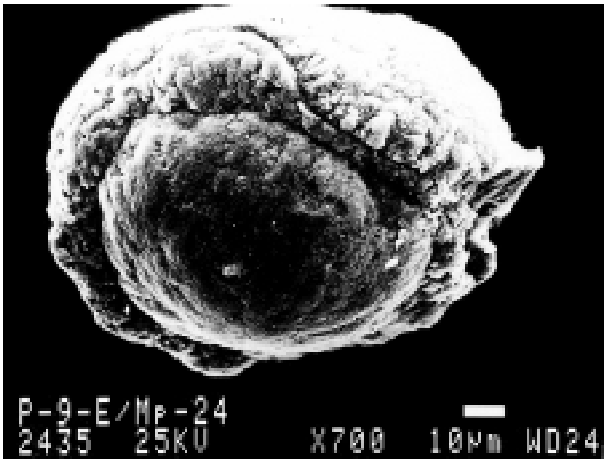

Fig. 3. Spheroidal uraninite overgrown by brannerite. ZV 2, SEM -SEI.

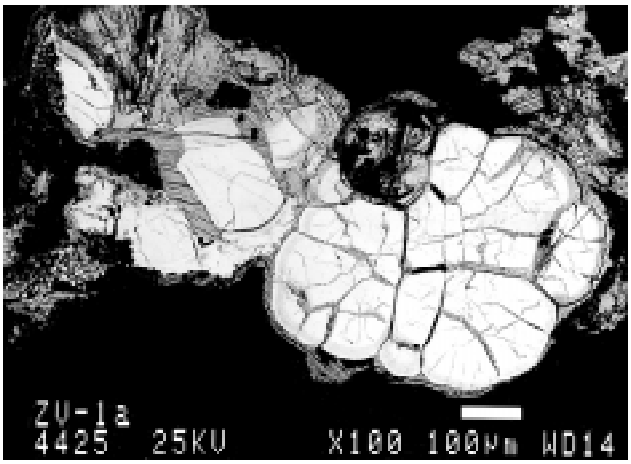

Fig. 4. Spheroidal aggregate of uraninite (white) in quartz (black) is replaced from the margin by zeunerite (light-grey). ZV 1a, SEM-BEI.

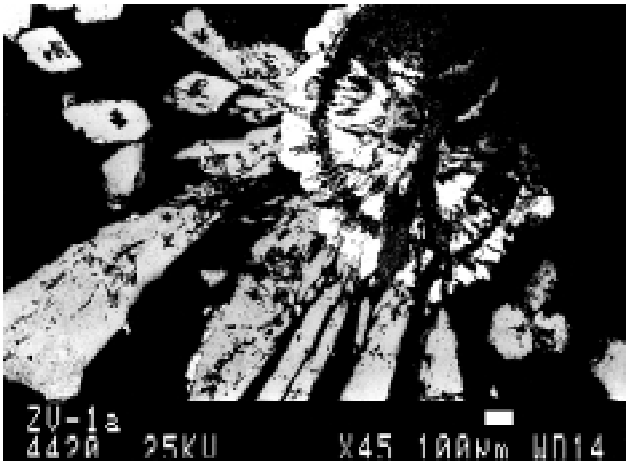

Fig. 5. Radial aggregate of brannerite crystals (grey) overgrowing on zonal uraninite (white) in quartz (black). ZV 1a, SEM-BEI.

Table 1: Chemical composition of uraninite.

Sample	Weight %							
	U	Pb	Fe	Si	Ca	Ti	O	Total
U_3O_8	84.8						15.2	100.0
ZV 1.1	85.2		1.5	0.6			12.8	100.1
ZV 1.2	80.2	1.6	0.5	0.1	0.2	0.5	11.7	94.8
ZV 1.3	79.8	1.5	0.6	0.1	0.1	0.6	11.7	94.4
ZV 1.4	78.7	1.6	0.6		0.2	0.6	11.4	93.1
ZV 1.5	76.9	1.6	1.0	0.1	0.2	0.5	11.4	91.7

Table 2: Chemical composition of brannerite and UTi_2O_6.

Sample	Weight %							At. prop.	
	U	Ti	Fe	Ca	Si	O	Total	U	Ti
UTi_2O_6	55.4	22.3				22.3	100.0	1.00	2.00
ZV 1.1	52.3	21.4	0.7	1.7		22.3	98.4	1.03	1.97
ZV 1.2	52.8	21.6	1.3	1.4		22.7	99.8	0.99	2.01
ZV 1.3	52.0	20.7	0.2	1.5	0.1	21.6	96.1	1.01	1.99
ZV 1.4	50.2	21.5	1.4	1.6	0.1	22.5	97.3	0.96	2.04
ZV 1.5	52.8	20.0	1.1	1.4		21.5	96.8	1.04	1.96
ZV 1.6	51.8	20.4	0.1	1.5	0.2	21.5	95.5	1.01	1.99
ZV 1.7	53.9	21.4	0.3	1.5	0.2	22.4	99.7	1.01	1.99

Brannerite UTi_2O_6 or $(U,Ca,Th,Y)[(Ti,Fe)_2O_6]$ is a frequent and abundant uranium mineral in the vein. It can be seen with the naked eye as black columnar crystals up to 3 mm long. Crystals often form radial aggregates (Fig. 5). They radially overgrow uraninite. They contain inclusions of xenotime-(Y) and rutile (Fig. 6). Chemical composition corresponds to the ratio U : Ti = 1 : 2 and brannerite contains admixtures of Fe, Ca and Si (Table 2).

Rutile TiO_2 forms irregular xenomorphic grains (10 µm up to 0.3 mm across). They are often associated with uraninite and xenotime-(Y). This rutile was formed due to metamictization and the following alteration of brannerite to Ti oxides, xenotime-(Y) and uraninite (Fig. 6). The rutile accompanied

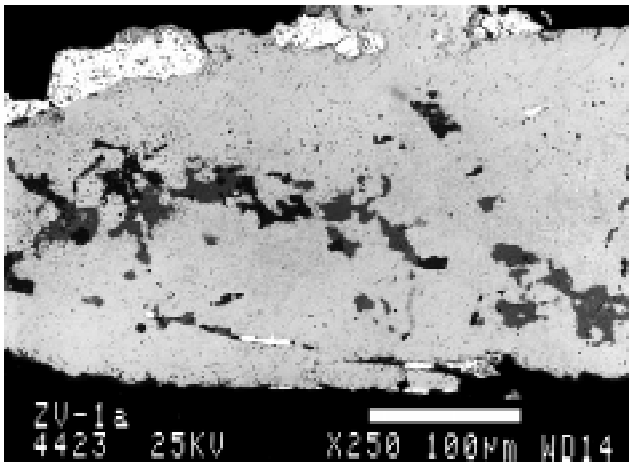

Fig. 6. Detail of spot from Fig. 5. Brannerite (light-grey) with admixture of rutile (dark-grey), xenotime-(Y) (grey) and overgrowing uraninite (white in upper part) is cut by veinlets of gold (white in central lower part). ZV-1a, SEM-BEI.

by xenotime-(Y) contains a homogeneous admixture of Fe and an increased content of Nb (1.1 wt. % Nb; Table 3).

Arsenopyrite FeAsS is relatively frequent and form aggregates macroscopically visible with crystals of radial texture from 1 to 5 mm long (Fig. 7). It fills interstices of the brannerite aggregates. Prismatic crystals and rhombic sections are visible under the polarizing microscope. Admixtures of Co, Ni and Sb were found (Table 4). Arsenopyrite with distinctly increased Co content (9 wt. %) corresponds to the Co variety of arsenopyrite — danaite (Fig. 8).

Glaucodot (Co,Fe,Ni)AsS forms grain aggregates and prismatic crystals often of radial texture in quartz (Fig. 7). They often show a cataclastic texture similar to arsenopyrite.

Table 3: Chemical composition of rutile.

	Weight %				
Sample	**Ti**	**Fe**	**Nb**	**O**	**Total**
TiO_2	59.9			40.1	100
ZV 1	58.7	0.5	1.1	39.7	100

Table 4: Chemical composition of arsenopyrite and Co-arsenopyrite (danaite).

	Weight %						
Sample	**Fe**	**Co**	**Ni**	**Sb**	**As**	**S**	**Total**
ZV-1	38.6	0	0	0	38.8	22.7	100.1
ZVH-1	34.8	0.8	0	0	45.4	18.9	99.9
ZVH-2	32.8	1.7	0.1	0	45.5	20.1	100.2
ZVH-3	32.9	1.9	0.1	0	45.2	19.6	99.7
ZVH-4	33.0	2.1	0.2	0.4	46.0	19.0	100.7
ZVH-5	32.7	2.1	0.2	0.7	45.7	19.5	100.9
ZVH-6	29.7	4.8	0.4	0	45.1	19.0	99.0
ZVH-25*	27.2	4.9	0.6	1.0	49.3	15.9	98.9
ZVH-26*	28.7	5.2	0.3	0	46.1	18.9	99.2
ZVH-24*	26.6	6.8	0.5	0	47.4	17.3	98.6
ZVH-23*	25.5	8.0	0.8	0	46.5	18.1	98.9
ZVH-22*	24.4	8.9	0.7	0	49.2	17.5	100.7
ZVH-7	23.4	9.1	2.0	0	47.9	18.7	101.1
ZVH-21*	23.1	10.6	0.4	0	46.5	18.3	98.9
	Atomic proportion on 3 atoms						
ZV-1	1.08	0	0	0	0.81	1.10	
ZVH-1	1.02	0.02	0	0	1.00	0.97	
ZVH-2	0.95	0.05	0	0	0.98	1.01	
ZVH-3	0.96	0.05	0	0	0.98	1.00	
ZVH-4	0.96	0.06	0.01	0.01	1.00	0.97	
ZVH-5	0.95	0.06	0.01	0.01	0.99	0.99	
ZVH-6	0.88	0.13	0.01	0	0.99	0.98	
ZVH-25*	0.84	0.14	0.02	0.01	1.13	0.85	
ZVH-26*	0.85	0.15	0.01	0	1.02	0.98	
ZVH-24*	0.81	0.20	0.01	0	1.07	0.91	
ZVH-23*	0.76	0.23	0.02	0	1.04	0.95	
ZVH-22*	0.72	0.25	0.02	0	1.09	0.91	
ZVH-7	0.69	0.25	0.06	0	1.05	0.95	
ZVH-21*	0.69	0.30	0.01	0	1.04	0.96	

*transitional zone of radial aggregate (see Fig. 7)

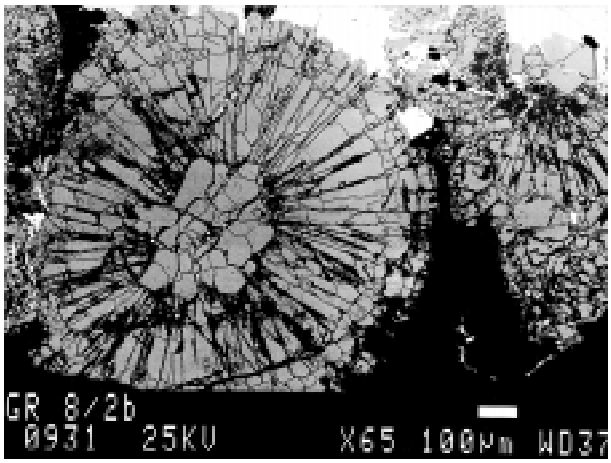

Fig. 7. Radial aggregate of zonal crystals of arsenopyrite and glaucodot. The centre of the aggregate is represented by cobaltite grains, the transitional zone by arsenopyrite and Co-arsenopyrite (danaite) and the external part by glaucodot. Bismuthite (white) forms the rim and veinlets in the aggregate. GR 8/2b, SEM-BEI.

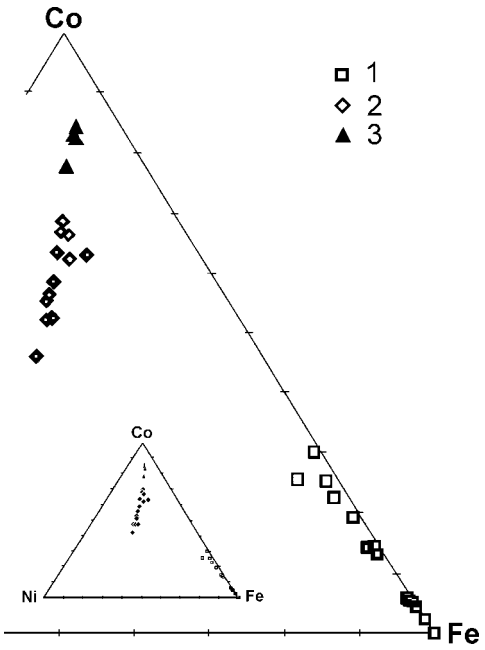

Fig. 8. Ternary diagram of Fe, Co and Ni content in arsenopyrite (1), glaucodot (2) and cobaltite (3).

Skeleton-shaped crystals of glaucodot can be seen frequently. It is lighter compared to arsenopyrite in reflected light. It shows strong anisotropy of blue and orange colour. Fissures of glaucodot are filled by bismuthinite, younger quartz, rarely also by carbonate. Radial aggregates are interesting from the genetic point of view. Euhedral cobaltite form their centre. Transitional zone is formed by arsenopyrite and danaite. Glaucodot forms a marginal part of the aggregate.

WDX analysis confirmed increased content of Ni in glaucodot (comparing to data of literature). However, the total of Fe + Ni does not exceed the Co content. The data obtained (Table 5, Fig. 8) correspond well to a Co content from 16 to 25 % Co given for glaucodot by Strunz (1970). Rudaschevsky in

Borischanskaya et al. (1981) gives for glaucodot ratio of Fe : Co from 65 : 35 to 35 : 65. It corresponds to a Fe content from 11.86 to 22.15 wt. % and Co content from 12.58 to 23.24 wt. % Co. Ratio of Fe : Co from 65 : 35 to 100 : 0 corresponding to less than 11.86 wt. % of Fe and from 23.24 to 35.41 wt. % of Co is given by Rudaschevsky in Borischanskaya et al. (1981) for alloclasite. The zonality of grains not visible under the polarizing microscope can be observed only with the scanning electron microscope and it was confirmed by WDX analysis (Table 5). Increase of cobalt in external zones was observed in the zonal aggregates of glaucodot. The central zone shows a low content of Co in glaucodot due to the cobalt bond in cobaltite. Variability of chemical composition is documented in the ternary diagram of Co-Fe-Ni sulphoarsenides (Fig. 8).

Cobaltite CoAsS forms irregular grain aggregates, rarely euhedral grains in the centre of radial aggregates of Co-Fe-Ni sulphoarsenides (Fig. 7). It shows high reflectivity, pinkish white colour and isotropy. Its chemical composition is documented in Table 6 and the ternary diagram in Fig. 8.

Pyrite FeS_2 forms rounded grains (up to 0.3 mm across) and their aggregates. Intergrowths of octahedral and pentagonal dodecahedron crystals are rare. They are more abundant in the external part of the vein with a decreased content of arsenopyrite, gold and uranium minerals.

Gold Au. Gold is visible even with the naked eye in the high-grade ore in the western section of the vein. It was found only after separation in the sample from the western part of the vein (135 grains). Grains from 2 to 100 μm (rarely up to 400 μm) can be observed under the polarizing microscope. The grains are oval, lobe-form or they fill fissures and intergranular space in older minerals. Section across octahedral crystals can rarely be seen (Figs. 9, 10). It occurs in quartz, uraninite, brannerite and rarely also in arsenopyrite, glaucodot and bismuthinite (Fig. 9). It overgrows, encloses and cuts previous minerals. For example uraninite from sample GR-6a/11 of 0.104 g weight contains 0.56 $g.t^{-1}$ Au. Intergrowths of uraninite and arsenopyrite from sample GR-6a/13 of 0.089 g weight contain 5.31 $g.t^{-1}$. The largest grains (over 100 μm), in oxidation products of the vein with abundant goethite and scorodite, are most probably of supergene origin. The content of the gold ranges from 773 to 999/1000 (Table 7a–b, Fig. 11).

Distribution of gold was also studied during the dressing. The abundance of gold grains, their size, composition and form were studied after grinding and separation (Table 8). The surface of the grains is different: flakes, sinuous, smooth or, elongated lobe-likes, isometric grains, rarely euhedral of octahedral form (Fig. 10).

Bismuth occurs rarely. It is associated with bismuthinite in intergranular space of glaucodot as irregular grains up to 50 μm across. Content of 99.8 wt. % Bi was confirmed by EDX analysis.

Bismuthinite Bi_2S_3 is mostly associated with glaucodot. It forms needle-like and tabular crystals in quartz (Fig. 12) or more frequently it fills fissures or intergranular space of aggregates of Co-Fe-Ni sulphoarsenides (Fig. 13). It shows reflectivity close to galena in the polarizing microscope, white colour and strong anisotropy. Prismatic sections also show longitudinal cleavage. An increased content of Sb (up to 11.6 wt. %) was observed. Its composition is close to horobetsuite. An increased content of Pb (up to 5.5 wt. %) was also found. Chemical composition is documented by Table 9 and by a ternary diagram of Bi–Sb–Pb minerals (Fig. 14).

Molybdenite MoS_2 was found only as a rare mineral. Disseminated flakes of molybdenite in quartz are up to 20 μm long and up to 5 μm across. It is closely associated with arsenopyrite and uraninite. In spite of the small size of grains, WDX analysis has confirmed the identification of molybdenite (Table 10).

Table 5: Chemical composition of glaucodot.

	Weight %						
Sample	**Fe**	**Co**	**Ni**	**Sb**	**As**	**S**	**Total**
ZVH-8	8.0	16.3	10.8	0	46.7	19.2	101.0
ZVH-9	7.5	18.3	8.9	0	44.2	19.2	98.1
ZVH-10	7.7	18.6	8.9	0	45.3	18.5	99.0
ZVH-11	7.6	18.9	9.4	0	45.4	18.4	99.7
ZVH-12	6.7	19.8	8.2	0	47.1	19.7	101.5
ZVH-13	7.0	20.0	8.8	0.1	46.0	17.7	99.6
ZVH-14	6.9	21.4	8.0	0	46.5	18.2	101.1
ZVH-15	6.8	22.3	6.5	0	46.6	19.2	101.4
ZVH-16	6.0	22.9	6.9	0	45.3	19.5	100.6
ZVH-17	7.9	23.9	5.8	0	45.3	17.1	100.0
ZVH-20*	6.0	24.0	5.8	0	45.6	19.2	100.6
ZVH-18	5.6	24.1	6.0	0	46.2	18.5	100.4
ZVH-19	5.3	24.5	5.6	0	45.6	18.6	99.6
	Atomic proportion on 3 atoms						
ZVH-8	0.24	0.46	0.30	0	1.03	0.98	
ZVH-9	0.23	0.52	0.25	0	0.99	1.01	
ZVH-10	0.23	0.53	0.25	0	1.02	0.97	
ZVH-11	0.23	0.54	0.27	0	1.01	0.96	
ZVH-12	0.20	0.55	0.23	0	1.03	1.00	
ZVH-13	0.21	0.57	0.25	0	1.03	0.93	
ZVH-14	0.20	0.60	0.23	0	1.03	0.94	
ZVH-15	0.20	0.62	0.18	0	1.02	0.98	
ZVH-16	0.18	0.64	0.19	0	0.99	1.00	
ZVH-17	0.24	0.68	0.17	0	1.02	0.90	
ZVH-20*	0.18	0.67	0.16	0	1.00	0.99	
ZVH-18	0.17	0.68	0.17	0	1.02	0.96	
ZVH-19	0.16	0.70	0.16	0	1.01	0.97	

*marginal zone of radial aggregate (see Fig. 7)

Table 6: Chemical composition of cobaltite.

	Weight %					
Sample	**Co**	**Fe**	**Ni**	**As**	**S**	**Total**
ZVH-28*	28.2	4.0	4.0	45.1	19.0	100.3
ZVH-27*	29.7	3.4	2.6	45.1	18.7	99.5
ZVH-29*	29.9	3.6	2.6	44.9	19.2	100.2
ZVH-30*	30.2	3.2	2.3	46.3	19.2	101.2
	Atomic proportion on 3 atoms					
ZVH-28*	0.79	0.12	0.11	1.00	0.98	
ZVH-27*	0.84	0.10	0.07	1.01	0.98	
ZVH-29*	0.84	0.11	0.07	0.99	0.99	
ZVH-30*	0.84	0.09	0.06	1.01	0.98	

*central zone of radial aggregate (see Fig. 7)

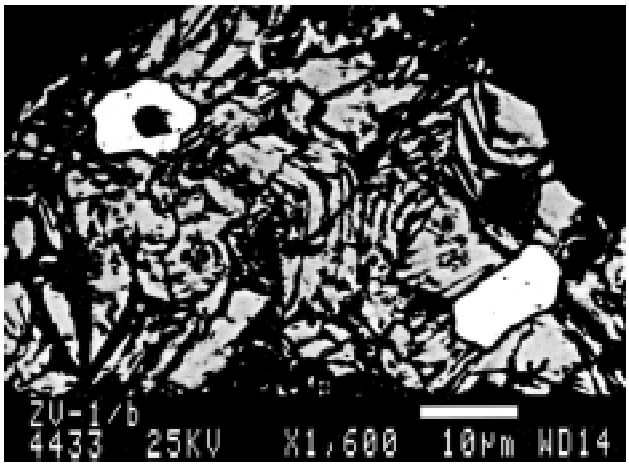

Fig. 9. Section of octahedral crystal of gold (white) in uraninite (grey). ZV 1b, SEM-BEI.

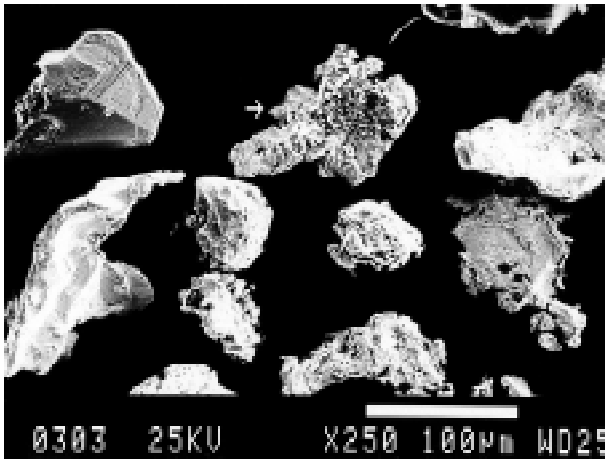

Fig.10. Separated gold grains from sample GR-6a-12/4. A fragment of gold octahedron can be seen on the left in the upper part. SEM-SEI.

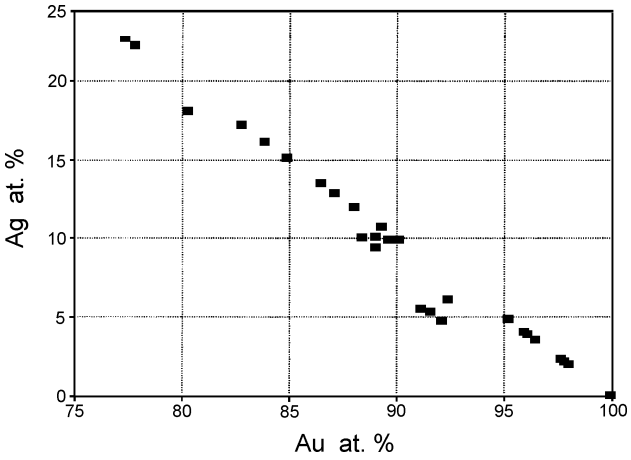

Fig. 11. Correlation plot of Au and Ag in gold.

Galena PbS small rare grains have been found in quartz in association with bismuthinite with increased Pb content (Fig. 12).

Tetrahedrite $Cu_{12}Sb_4S_{13}$ is rare. It forms irregular grain aggregates and veinlets in quartz associated with arsenopyrite. Its chemical composition is documented by Table 11.

Table 7a: Chemical composition of gold (WDX analyses).

	Weight %						Atomic propor. on 1000				
Sample	**Au**	**Ag**	**Hg**	**Cu**	**Bi**	**Total**	**Au**	**Ag**	**Hg**	**Cu**	**Bi**
ZV 1.1	92.9	3.1	2.6	0	0.9	99.5	911	56	25		8
ZV 1.2	95.2	2.7	2.0	0.3	0.4	100.6	921	48	19	9	4
ZV 1.3	94.3	3.0	2.4	0.1	0.6	100.4	915	53	23	3	6
ZV 1 h	93.2	5.7	0.5	0		99.4	896	99	5		
ZV 2 h	91.6	5.7	0.9	0		98.2	890	101	8	1	
ZV 3 h	86.4	10.7	1.7	0		98.8	803	181	15	1	
ZV 4 h	91.2	5.7	0.6	0.3		97.8	884	100	6	10	
ZV 5 h	96.5	3.5	0.8	0.2		101.0	924	61	8	7	
ZV 6 h	92.7	5.4	0.6	0.3		99.0	890	94	6	10	

Table 7b: Chemical composition of gold (EDX analyses).

				At.p./1000	
Sample	**Au**	**Ag**	**Total**	**Au**	**Ag**
ZV 1.4	98.7	1.3	100.0	977	24
ZV 1.5	98.9	1.2	100.1	978	22
ZV 1.6	99.0	1.1	100.1	980	20
ZV 7 h	97.7	2.3	100.0	959	41
ZV 8 h	97.8	2.2	100.0	961	39
ZV 9 h	85.8	13.4	99.2	778	222
ZV 10h	85.9	13.8	99.7	774	226
ZV 11h	93.8	6.2	100.0	893	107
ZV 12h	99.9	0.1	100.0	999	1
ZV 13h	89.8	10.2	100.0	828	172
ZV 14h	93.1	7.0	100.1	880	120
ZV 15h	91.1	8.9	100.0	849	151
ZV 16h	97.3	2.7	100.0	952	48
ZV 17h	92.5	7.5	100.0	871	129
ZV 18h	96.9	2.7	99.6	951	49
ZV 19h	98.0	2.0	100.0	964	36
ZV 20h	87.0	14.0	101.0	773	227
ZV 21h	93.5	5.6	99.1	901	99
ZV 22h	90.5	9.6	100.1	838	162
ZV 23h	92.1	7.9	100.0	864	136

Table 8: Distribution of gold separated from ground samples.

Sample	**gold grains**	**size of grains (µm)**	**Au on 1000**	**form of gold**
GR-6a/11	37	30-300	910-920	flakes, isometric
GR-6a/12	26	30-200	860-970	grains, elongated
GR-6a/13	42	30-150	860-990	lobe-like, sinuous

Apatite $Ca_5[F|(PO_4)_3]$ forming short columnar crystals (0.1×0.08 mm) accompanies ore minerals, sericite (aggregates up to 1 mm across) and chlorite in the quartz vein.

Xenotime-(Y) $Y[PO_4]$ can be observed as small admixtures in brannerite (Fig. 6). It fills fissures and cavities of concentric colloform aggregates of uraninite accompanied by brannerite and quartz (Fig. 15). Besides the dominant elements (Y and P) the heavy rare earth elements (HREE) from Gd to Yb with ionic radii close to Y are present (Table 12).

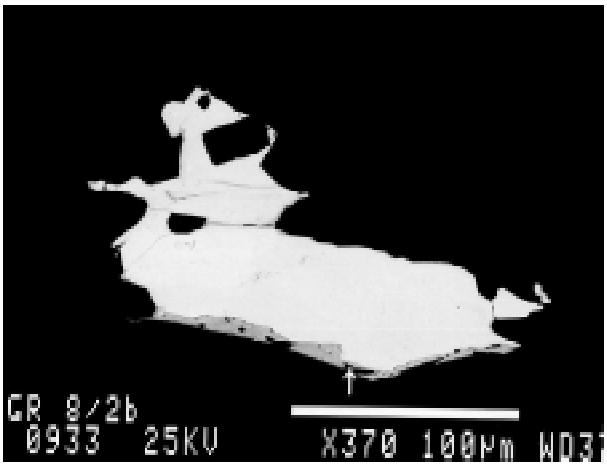

Fig. 12. Tabular bismuthinite with small grains of galena (marked with arrow) in quartz. GR 8/2b, SEM-BEI.

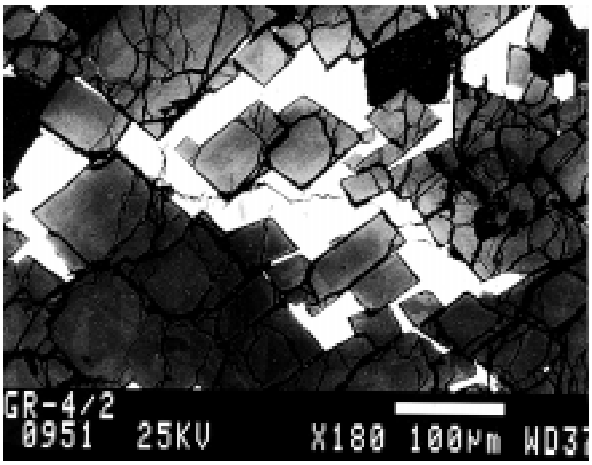

Fig. 13. Bismuthite in intergranular space and fissures of zonal arsenopyrite and glaucodot. GR 4/2, SEM-BEI.

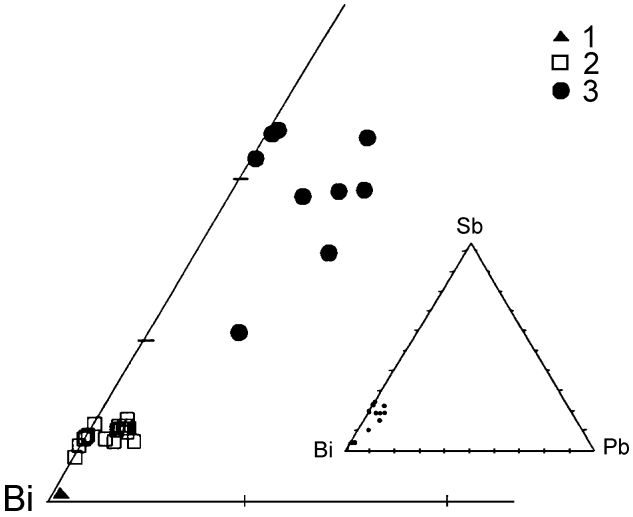

Fig. 14. Ternary diagram of Bi, Sb and S in bismuth (1), bismuthinite (2) and Sb-bismuthinite (3).

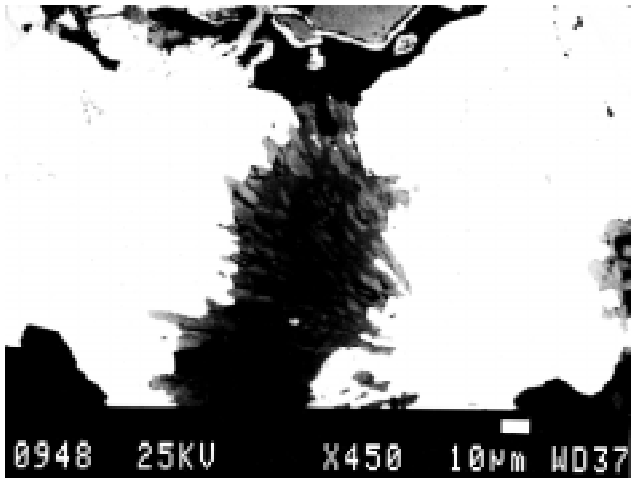

Fig. 15. Needle-like aggregate of xenotime-(Y) forms veinlet in uraninite. GR 2/1. SEM-BEI

There is a higher proportion of uranium than thorium in xenotime-(Y) comparing to monazite-(Ce).

Monazite-(Ce) $Ce[PO_4]$ is the main mineral of light rare earth elements (LREE). Disseminated grains of monazite-(Ce) up to 0.2 mm across can be observed in mineralized and altered rocks. Th content in monazite-(Ce) ranges from 0.9 to 4.5 wt. % (Table 13).

Quartz SiO_2 is the dominant gangue mineral. It is of brown colour. Grains are mostly xenomorphic, of mosaic texture, from 0.05 to 0.1 mm rarely up to 1 mm across and they show undulatory extinction. Prismatic crystals with pyramidal tops can also be seen.

Tourmaline $Na(Mg,Fe,Mn,Li,Al)_3Al_6(BO_3)_3(OH,F)_4[Si_6O_{18}]$, forming columnar crystals (from 0.03 to 0.4 mm long) of green colour with typical pleochroism, is abundant mainly in hydrothermally altered phyllite with monazite-(Ce).

Goethite a-FeOOH and **limonite** occur as colloform botryoidal aggregates from 0.05 to 2 mm across in fissures and cavities. They replace pyrite, and pseudomorphs of goethite after euhedral pyrite can be observed.

In the outcrops, the vein is characterized by the presence of iron hydroxides, and by the presence of secondary minerals of yellow and yellowish-green colour. These are weathering products of uranium minerals and arsenopyrite alteration.

Trögerite $(H_3O)_2[UO_2|AsO_4]_2.6H_2O$? forms yellow coatings of samples with abundant uraninite, brannerite and arsenopyrite. It also forms pseudomorphs after colloform and spheroidal uraninite up to 1 mm across. However EDX analysis of mineral with moderately increased content of Fe does not exclude the presence of kahlerite $Fe[UO_2|AsO_4]_2.12H_2O$ or metakahlerite (Table 14).

Zeunerite $Cu[UO_2|AsO_4]_2.10H_2O$ is rare in strongly weathered samples with goethite. It is characterized by deep green internal reflection and distinct cleavage under the polarizing microscope (Fig. 16). It is in close paragenetic association with goethite. The identification of zeunerite was confirmed by EDX analysis (Table 15).

Scorodite $Fe^{3+}[AsO_4].2H_2O$ is often associated with

Table 9: Chemical composition of bismuthinite.

	Weight %						Atomic proportion on 3 atoms				
Sample	**Bi**	**Cu**	**Pb**	**Sb**	**S**	**Total**	**Bi**	**Cu**	**Pb**	**Sb**	**S**
ZV 17h	79.1	0.3		2.3	17.9	99.6	1.97	0.02		0.10	2.91
ZV 18h	78.6	0.4	1.6	2.1	17.5	100.2	1.97	0.04	0.04	0.09	2.86
ZV 7 h	78.4			1.8	20.6	100.8	1.82			0.07	3.11
ZV 5 h	78.3	0.4	1.3	1.8	17.0	98.8	2.01	0.03	0.03	0.08	2.85
ZV 4 h	78.2	0.4	0.8	1.8	17.2	98.4	2.00	0.03	0.02	0.08	2.87
ZV 6 h	78.1			1.6	17.2	96.9	2.03			0.07	2.90
ZV 16h	78.0	0.5	1.4	2.2	17.6	99.7	1.95	0.04	0.04	0.09	2.87
ZV 14h	77.7	0.5	1.3	2.3	17.7	99.5	1.95	0.04	0.03	0.10	2.88
ZV 9 h	77.6	0.5	1.6	2.2	17.8	99.7	1.93	0.04	0.04	0.09	2.89
ZV 15h	77.5	0.5	1.1	2.1	17.6	98.8	1.95	0.04	0.03	0.09	2.89
ZV 10h	77.5	0.5	1.2	2.2	17.8	99.2	1.93	0.04	0.03	0.09	2.90
ZV 8 h	77.5			1.3	20.9	99.7	1.79			0.05	3.16
ZV 13h	77.3	0.6	1.3	2.4	17.5	99.1	1.94	0.05	0.03	0.10	2.87
ZV 12h	77.0	0.5	1.3	2.1	17.7	98.6	1.94	0.04	0.03	0.09	2.90
ZV 11h	76.5	0.5	1.1	2.2	17.6	97.9	1.93	0.04	0.03	0.09	2.91
ZV 2 h	75.6			1.8	22.1	99.5	1.70			0.07	3.23
ZV 3 h	75.3			1.9	21.7	98.9	1.71			0.07	3.21
ZV 19h	72.9	0.7	3.8	5.1	18.2	100.7	1.77	0.05	0.09	0.21	2.88
ZV 23h	68.2	0.5	2.9	9.7	18.6	99.9	1.62	0.04	0.07	0.39	2.88
ZV 24h	67.9			10.6	22.6	101.1	1.46			0.39	3.15
ZV 26h	67.3			11.6	22.4	101.3	1.44			0.43	3.13
ZV 21h	67.0	0.6	4.4	9.9	18.9	100.8	1.57	0.05	0.10	0.40	2.88
ZV 25h	66.9			11.4	22.4	100.7	1.44			0.42	3.14
ZV 20h	66.8	0.5	5.5	7.6	21.2	101.6	1.48	0.04	0.12	0.29	3.07
ZV 22h	66.4	0.5	5.5	10.0	18.2	100.6	1.59	0.04	0.13	0.41	2.83
ZV 27h	62.6	0.5	4.2	11.3	22.4	101.0	1.34	0.03	0.09	0.41	3.13

Table 10: Chemical composition of molybdenite.

	Weight %			Atomic prop.	
Sample	**Mo**	**S**	**Total**	**Mo**	**S**
ZV 12b.1	56.8	44.9	101.7	0.89	2.11
ZV 12b.2	55.4	44.1	99.5	0.89	2.11
ZV 12b.3	58.7	44.5	103.2	0.92	2.08
ZV 12b.4	56.7	45.6	102.3	0.88	2.12

Table 11: Chemical composition of tetrahedrite.

	Weight %						
Sample	**Cu**	**Fe**	**Zn**	**Sb**	**As**	**S**	**Total**
ZV 4/2	38.3	4.9	1.8	31.6	0.2	24.1	100.9
ZV 4/3	38.4	4.7	2.0	31.6	0.1	23.5	100.3
	Atomic proportion on 29 atoms						
ZV 4/2	10.1	1.5	0.5	4.3		12.5	
ZV 4/3	10.2	1.4	0.5	4.4		12.4	

trögerite (?). It forms light-green and yellow-green powder coatings in samples with abundant arsenopyrite. It replaces arsenopyrite (Fig. 17). Its identification was confirmed by EDX analysis (Table 16).

Table 12: Chemical composition of xenotime-(Y).

	Weight %						
Sample	**Y**	**Gd**	**Dy**	**U**	**P**	**O**	**Total**
YPO_4	48.4				16.8	34.8	100
ZV 1	28.2	5.3	7	0.9	21.4	37.2	100
	Atomic proportion on 2 atoms						
ZV 1	0.58	0.06	0.08	0.01	1.27		

Association of elements

The uranium accumulation in Zimná Voda is accompanied by distinctly increased contents of Au, B, La and Y (Table 17). The average content of Au in the whole vein is 25, 28 ppm and maximal content of Au reaches 164 ppm. Au contents range from 0.11 to 17. 8 ppm in the surrounding rocks and from 15 to 40 cm from vein.

Moderately are increased contents of Ag, Co, Cu, Mo, Ni, Pb, W and Zr. Quartz veins with U-Au-REE mineralization in the Slovenské rudohorie Mts. cut the Early Paleozoic sequences. They show significant enrichment with U, Au, Cu, Pb, Ca, Y, P, Th, Ag, Co, Sr, La and Mo compared to black phyllites and lydites (Rojkovič et al. 1995). This enrichment

Table 13: Chemical composition of monazite-(Ce).

	Weight %											
Sample	**Ce_2O_3**	**La_2O_3**	**Pr_2O_3**	**Nd_2O_3**	**Sm_2O_3**	**Gd_2O_3**	**ThO_2**	**Y_2O_3**	**SiO_2**	**CaO**	**PbO**	**P_2O_5**	**Total**
ZV 4p.1	31.6	15.3	5.2	14.0	2.8	2.2	1.6		0.6			26.1	99.4
ZV 4p.2	25.3	7.60	5.3	19.4	5.3	3.1	4.5		0.9			26.7	98.0
ZV 4p.3	31.5	12.6	4.8	16.7	3.4	2.9			0.3			27.8	100.1
ZV 4p.4	30.8	14.6	5.1	15.1	3.5	2.5	1.2		0.5			26.4	99.8
ZV 4p.5	28.3	13.2	4.7	15.9	3.7	2.5	2.5		0.7			25.9	97.4
ZV 4p.6	27.8	12.2	4.8	11.1	2.6	2.7	1.2	1.9	0.3	0.7	0.3	31.2	96.9
ZV 4p.7	29.3	12.7	4.7	12.9	2.9	3.0	0.9	2.0	0.2	0.4	0.2	31.0	100.2
ZV 4p.8	28.0	12.6	5.0	12.7	3.0	3.2	1.5	1.8	0.3	0.5	0.3	29.6	98.4
ZV 4p.9	29.0	11.6	5.2	13.9	2.6	2.5	2.5	2.0	0.7	0.5	0.2	28.5	99.1
ZV 4p.10	28.3	14.2	4.5	12.6	2.8	2.8	1.3	1.9	0.3	0.4		29.2	98.2
	Atomic proportion on 2 atoms												
	Ce	La	Pr	Nd	Sm	Gd	Th	Y	Si	Ca	P	R^{+3}	O^{-2}
ZV 4p.1	0.49	0.24	0.08	0.21	0.04	0.03	0.02				0.93	2.04	4
ZV 4p.2	0.39	0.12	0.08	0.29	0.08	0.04	0.04				0.96	2.01	4
ZV 4p.3	0.47	0.19	0.07	0.24	0.05	0.04					0.96	2.03	4
ZV 4p.4	0.47	0.22	0.08	0.23	0.05	0.04	0.01				0.94	2.04	4
ZV 4p.5	0.45	0.21	0.07	0.24	0.05	0.04	0.02				0.94	2.03	4
ZV 4p.6	0.40	0.18	0.07	0.16	0.04	0.04	0.01	0.04			1.04	1.97	4
ZV 4p.7	0.42	0.18	0.07	0.18	0.04	0.04	0.01	0.04			1.02	1.99	4
ZV 4p.8	0.41	0.19	0.07	0.18	0.04	0.04	0.01	0.04			1.00	1.99	4
ZV 4p.9	0.43	0.17	0.08	0.2	0.04	0.03	0.02	0.04			0.98	2.01	4
ZV 4p.10	0.42	0.21	0.07	0.18	0.04	0.04	0.01	0.04			1.00	2.00	4

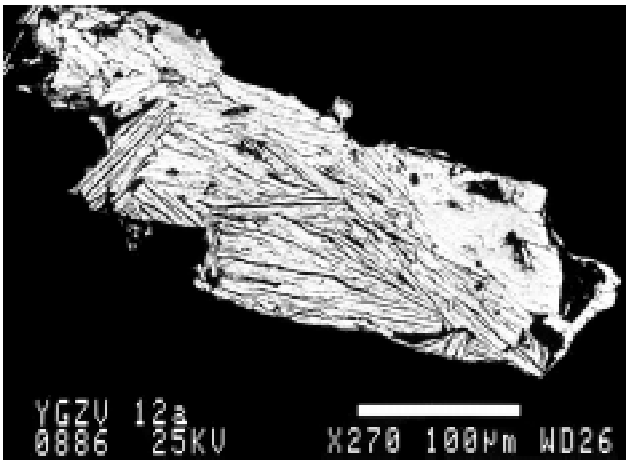

Fig. 16. Aggregate of zeunerite (white). ZV 12a, SEM-SEI.

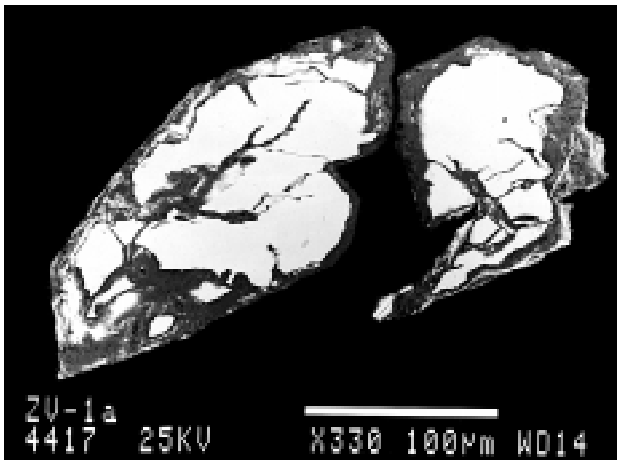

Fig. 17. Scorodite (grey) replaces arsenopyrite (white) from margin and along fissures. ZV 1a, SEM-BEI.

reflects the presence of apatite, xenotime-(Y), uraninite, gold and arsenopyrite in veins. W also shows a local increase.

Origin of mineralization

Quartz veins with U-Au-REE mineralization occur close to the Humel Granite but also in proximity to the Hnilec Granite (Varček 1975; Rojkovič & Novotný 1993). They show a spatial and partly also material relationship to the Gemeric granites with increased content of U, Sn, Th and B. The important sources of metals were probably the surrounding sediments such as black phyllites, lydites and associated phosphates (Rojkovič et al. 1995). Black phyllites and lydites were a probable source of Au, Ag, Mo, Cu (partly U), and associated phosphates were a probable source of REE in veins. Sediments with increased contents of organic matter, P, U, W, Mo and REE are the probable source of the similar vein U-Au mineralization near Hoehensteinweg in Germany (Dill 1982). The copper vein mineralization is accompanied by uraninite,

Table 14: Chemical composition of trögerite (?).

Sample	Weight % U	Fe	As	O	Total
$U_2As_2O_{20}H_{18}$[1]	49.4	0.0	15.5	33.2	+H 1.9
$FeU_2As_2O_{24}H_{24}$[2]	43.7	5.1	13.7	35.2	+H 2.2
$FeU_2As_2O_{20}H_{16}$[3]	46.8	5.5	14.7	31.4	+H 1.6
YZV 1	55.2	2.5	22.3	20.1	100.1
	Atomic proportion on 5 atoms				
	U	Fe	As		Total
YZV 1	2.02	0.39	2.59		5.00

[1]trögerite, [2]kahlerite, [3]metakahlerite

Table 15: Chemical composition of zeunerite.

Sample	Weight % Cu	U	P	As	O	Total
$CuU_2P_2O_{22}H_{20}$[1]	6.5	48.9	6.4		36.1	+H 2.1
$CuU_2P_2O_{20}H_{16}$[2]	6.8	50.8	6.6		34.1	+H 1.7
$CuU_2As_2O_{22}H_{20}$[3]	6.0	44.8		14.1	33.2	+H 1.9
$CuU_2As_2O_{20}H_{16}$[4]	6.2	46.4		14.6	31.2	+H 1.6
ZV 12.1	1.5	57.8	0.2	20.5	14.9	94.9
ZV 12.2	1.1	58.3	0.1	21.7	15.1	96.3
ZV 12.3	1.0	59.7	0.1	22.3	15.5	98.6

[1]torbernite, [2]metatorbernite, [3]zeunerite, [4]metazeunerite

Table 16: Chemical composition of scorodite.

Sample	Weight % Fe	As	P	O	Total	Atomic prop. Fe	As
$FeAsO_6H_4$	24.2	32.5		41.6	+H 1.75		
ZV 1	28.9	35.8	1.7	33.7	100.1	1.04	0.96

Table 17: Contents of trace elements (in ppm) in vein and wall rocks.

	Ag	Au	B	Corg	Co	Cu	La	Mo	Ni	Pb	Ti	U	V	W	Zr	Y
a	6	25	692	281	139	44	421	18	40	43	4075	1336	79	224	352	421
m	53	164	2880	800	960	134	1800	106	106	234	6050	11852	155	270	836	1910

a—average (Au from 43, the others from 10 samples), m—maximum

brannerite, molybdenite and gold in Mitterberg in Austria. It is a mobilization product of low-grade stratabound uranium mineralization in the Permian "Violet Serie" (Paar 1976).

The association of minerals such as uraninite, brannerite, molybdenite, tourmaline, apatite and monazite-(Ce) represent the older mineralization in the aureole of the Humel Granite Massif. Sulphidic minerals as arsenopyrite, glaucodot, cobaltite, tetrahedrite, bismuth, bismuthinite and galena represent the younger phase of mineralization. Characteristic is accumulation of Co–Fe–Ni sulphoarsenides (arsenopyrite, glaucodot, cobaltite) and bismuth minerals. Mineralization of the U-Au-Bi-Co-REE association was not described yet in the Western Carpathians.

The xenotime-(Y) is distinctly younger than the uranium mineralization and apatite in the vein studied. Remobilized xenotime-(Y) is often formed by release of Y and HREE from the uraninite lattice and by the following reaction with the mobile phosphates (Oberthür 1987).

Varček (1975) presumed a temperature of vein uranium mineralization in the Spišsko-gemerské rudohorie Mts. from 330 to 220 °C according to decrepitation temperatures. The homogenization temperature of fluid inclusions in quartz associated with uranium mineralization in Zimná Voda gives T_{hom} from 300 to 450 °C and T_{hom} from 240 to 280 °C for quartz associated with younger sulphides. Uranium is probably transported in chloride and fluoride complexes at temperatures from 300 to 600 °C (Redkin et al. 1989).

Gemeric granites show large isotopic heterogeneity. The strontium isotopes were homogenized in the period from 270 to 223 Ma and standard interpretation identifies the time of homogenization with the time of granite intrusion. The younger (Cretaceous) age data are rather a result of the later alterations than polyphase origin (Kovách et al. 1986; Cambel et al. 1990). However Rb-Sr dating 101 ± 5 Ma of Rochovce Granite (Kovách et al. 1986) with disseminated U-Ti-REE mineralization confirms the Cretaceous age of granite. As reliable U-Pb dating of vein uranium mineralization is missing neither its Permian nor its Cretaceous age can be excluded.

Goethite, limonite and scorodite were formed during supergene processes. Gold was mobilized and large grains were formed.

Acknowledgments: Many thanks are due to rock and mineral analysis, SEM photographs to Pavol Siman, Patrik Konečný, František Caňo and Jozef Stankovič from Geological Survey in Bratislava, Ľubica Puškelová, Júlia Kotulová and Ivan Križáni of Geological Institute of the Slovak Academy of Sciences in Bratislava. This study was partly supported by Slovak Grant Agency by Project GA 2 1082: "Hercynian magmatism and rare element mineralization in the Western Carpathians". This paper is contribution to IGCP Project No. 373 "Correlation, Anatomy and Magmatic-Hydrothermal Evolution of Ore-Bearing Felsic Igneous Systems in Eurasia".

References

Bajaník Š., Vozárová A. & Reichwalder P., 1981: Lithostratigraphic classification of Rakovec Group and Late Paleozoic in Spišsko-gemerské rudohorie (ore mountains). *Geol. Práce, Spr.*, 75, 27–56 (in Slovak, English summary).

Bajaník Š., Ivanička J., Mello J., Reichwalder P., Pristaš J., Snopko L., Vozár J. & Vozárová A., 1984: Geological map of Slovenské rudohorie Mts., eastern part, 1:50,000, *GÚDŠ,* Bratislava.

Borischanskaya S.S, Vinogradova R.A. & Krutov G.A., 1981: Mineraly nikeľa i kobaľta. *Izd. Moskovskogo universiteta*, Moskva, 1–220 (in Russian).

Cambel B., Kráľ J. & Burchart J., 1990: Isotope geochronology of the Western Carpathians crystalline complexes. *VEDA*, Bratislava, 1–183 (in Slovak).

Dill H., 1982: Geologie und Mineralogie des Uranvorkommens am Hoehensteinweg bei Poppenreuth (NE-Bayern) — Ein Lagerstaettenmodell. *Geol. Jb. (Hannover),* 50, 83.

Faryad S. W., 1991: Pre-Alpine metamorphic events in Gemeric Unit. *Miner. slovaca*, 23, 395–402.

Grecula P., 1982: Gemericum — segment of the Paleotethyan riftogenous basin. *Miner. slovaca, Monografia* (Bratislava), 1–263 (in Slovak).

Ivanička J., Snopko L., Snopková P. & Vozárová A., 1989: Gelnica Group-Lower Unit of Spišsko-gemerské rudohorie Mts. (West Carpathians), Early Paleozoic. *Geol. Carpathica,* 40, 483–501.

Kovách A., Svingor E. & Grecula P., 1986: Rb-Sr izotopic ages of granitoids from the Spišsko-Gemerské rudohorie Mts. Western Carpathians. Eastern Slovakia. *Miner. slovaca*, 18, 1–14.

Novotný L. & Čížek P., 1979: New occurrence of uranium-gold mineralisation to the south of Prakovce village in Spišsko-gemerské rudohorie Mts. (Eastern Slovakia). *Miner. slovaca*, 11, 188–190 (in Slovak, English abstract).

Oberthür T., 1987: Mineralogy and geochemistry of phosphate minerals and brannerite from the proterozoic Carbon Leader Reef gold and uranium placer deposit, Witwatersrand, South Africa. *Monograph. Series on Mineral Deposits, Gebrüder Borntraeger,* Berlin-Stuttgart, 27, 129–142.

Paar W., 1976: Telluride der Gold-Nasturan Paragenese von Mitterberg (Salzburg). *Neu. Jb. Mineral., Mh.,* 193–202.

Redkin A.F., Savelyeva N.I., Sergeyeva E.I., Omelyanenko B.I., Ivanov I.P. & Khodakovsky I.L., 1989: Investigation of uraninite ($UO_{2(c)}$) solubility under hydrothermal conditions. *Sci. Géol., Bull.,* 42, 329–334.

Rojkovič I. & Novotný L., 1993: Uranium mineralization of Gemericum (Western Carpathian). *Miner. slovaca*, 25, 368–370 (in Slovak, English abstract).

Rojkovič I., Puškelová Ľ., Khun M. & Medveď J., 1995: U-REE-Au in veins and black shales of the Gemeric Unit, Slovakia. In: Pašava J., Kříbek B. & Žák K., (Eds.): Mineral deposits: From their origin to their environmental impacts. *A. A. Balkema*, Rotterdam, Brookfield, 789–792.

Strunz H., 1970: Mineralogische Tabellen. *Akademische Velagsgesellschaft, Geest & Portig K.-G.,* Leipzig 1–621.

Varček C., 1975: Mineralogical investigation of uranium mineralization in the central part of the Spišsko-gemerské rudohorie Mts., *Manuscript, URANPRES* Spišská Nová Ves, 1–214 (in Slovak).

Vozárová A. & Ivanička J., 1993: Lithogeochemistry of Early Paleozic metasediments in Southern Gemericum. *Západ. Karpaty, Sér. Mineral., Petrogr., Geochém., Metalogen.,* 16, 116–149 (in Slovak, English summary).